Simulation and experimental study of household R290 heat pump tumble dryer

Zhuang Chen[a], Shuangquan Shao[a *], Jiajun Zhao[b], Lianyu Shan[a,b], Shurong Zhang[b]

[a]School of Energy and Power Engineering, Huazhong University of Science and Technology, Wuhan 430074, China.
[b]Xiaomi Smart Appliances (Wuhan), Co., Ltd., Wuhan 430070, China.

Abstract

Heat pump clothes dryers have become a core focus for energy-saving upgrades in household appliances, thanks to their high energy efficiency and low-temperature drying features. To address safety and efficiency challenges of R290 heat pump dryers under compact design constraints, this study conducts systematic research on closed-cycle heat pump tumble dryer systems with eco-friendly R290 via integrated simulation and experiments. A quasi-steady-state model for closed-cycle systems is proposed, based on reverse enthalpy marching mechanisms coupled with the particle swarm optimization (PSO) algorithm. Prototype validation confirms model reliability, with average temperature prediction discrepancies 0.5 K. Combining thermodynamics with heat-mass transfer coupling, the study explores how compressor frequency, airflow rate, and other factors affect specific moisture extraction rate (*SMER*) and moisture extraction rate (*MER*). Optimizing compressor frequency boosts *MER* by 62.9% (1.26→2.05 kg/h) and *SMER* by 13.0% (2.23→2.52 kg/kWh). Within the test range, the *MER* decreases with increasing air volume flow rate (1.80→1.86 kg/h), while the *SMER* increases with increasing air volume flow rate (2.21→2.49 kg/kWh). This research provides a novel modeling paradigm for heat pump dryers and offers theoretical/optimization support for high-safety R290 engineering design.

Keywords: R290; Closed heat pump drying; Simulation and experiment; Moisture evaporation rate;

1. Introduction

With the emergence of new consumerism, global consumers have growing demands for clothing care quality, fueling increased adoption of household drying equipment. Clothes dryers—widely used in Europe and North America—reached penetration rates of 31.5% and 76.2% respectively in 2019 [1-2]. In the United States, 64% of residential dryers rely on direct electric heating, which typically features low energy efficiency. Per the International Energy Agency (IEA), dryers account for 3-6% of total household energy consumption in European and American residences [3]. Closed-cycle vapor-compression heat pump (VCHP) systems, based on the reverse Carnot cycle, recover waste heat from humid air via drum evaporators and are regarded as a core solution to transform traditional drying methods [4].

Currently, commercial heat pump dryers primarily use R134a or R404A. Their high global warming potential (GWP) conflicts sharply with emission reduction requirements in the Kigali Amendment [5]. Propane (R290)—a natural refrigerant with an ozone depletion potential (ODP) of 0 and a 100-year GWP (GWP_{100}) of 0—boasts favorable thermodynamic properties and is recognized as one of the most promising alternatives to conventional fluorinated refrigerants [6-7]. Shen et al. [8] conducted experimental studies on R290 as a replacement for R134a in heat pump water heaters. Results demonstrated that under optimal efficiency conditions, R290 not only enabled compatibility with compressors of smaller displacement capacities but also reduced the system refrigerant charge to merely 50% of that required for R134a. Similarly, Joudi et al. [9]

E-mail address: shaoshq@hust.edu.cn

performed experimental investigations on substituting R22 with R290 in heat pump systems, yielding analogous conclusions.

Although R290 has been increasingly adopted in European household heat pump dryers, its safe implementation under compact design constraints remains a key engineering challenge. Existing studies predominantly focus on refrigerant substitution, while systematic modeling and performance optimization for low-charge (<0.15 kg) closed-cycle systems are still insufficient [10]. To address this gap, the present work carries out a combined simulation and experimental investigation on an R290 heat pump tumble dryer. A quasi-steady-state model based on reverse enthalpy marching coupled with PSO is proposed to accurately predict heat pump system behavior. Furthermore, by investigating the heat and moisture transfer process within the drum during the drying cycle, the effects of critical operating parameters on drying performance are elucidated, providing insights into efficiency improvement under safety-limited conditions. This study offers a methodological framework and optimization guidance for the development of high-safety and high-efficiency R290-based dryer systems.

2. Methodology

2.1. System description

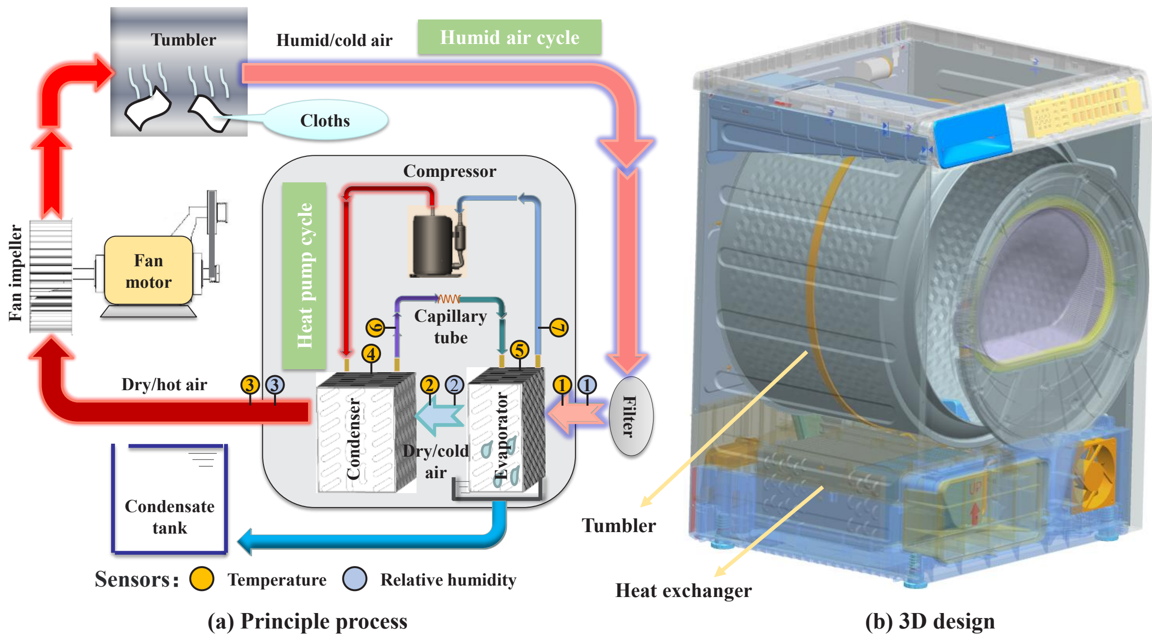

Figure 1. Closed heat pump tumble clothes dryer: (a) working principle process. (b) 3D design

Fig. 1 illustrates the operational principle and 3D design of a closed heat pump tumble dryer. High-temperature, low-humidity air from the condenser outlet is blown into the tumbler via the circulating fan, where it undergoes heat and moisture exchange with the clothes to be dried. After absorbing moisture from the garments, the air turns into a low-temperature, high-humidity state, passes through the mesh filter, and flows into the evaporator. Inside the evaporator, the air is cooled and dehumidified, with the generated condensate draining into the water tank. The dehumidified air exiting the evaporator then exchanges heat with the condenser, transforming back into high-temperature, low-humidity air that is blown into the tumbler again to initiate a new cycle. Owing to space limitations in the dryer's heat pump system compartment, the entire heat pump cycle system is designed with compact dimensions and a minimal refrigerant charge, usually employing a capillary tube for throttling.

2.2. Heat pump tumble dryer model

To streamline the complexity of the heat pump tumble dryer model, the following rational assumptions are adopted in the modeling process:

(1) The entire system and its constituent components operate under steady-state conditions.
(2) The refrigerant is uniformly distributed throughout the heat pump system.
(3) Key clothing parameters (e.g., moisture, specific heat) are uniform throughout the drying chamber.

2.2.1. Compressor and circulation fan models

Based on the measured data from compressor manufacturers, a data-driven model of compressor refrigerant flow (m_{ref}) and output power (P_{HP}) is constructed using the 15-factor method:

$$[m_{ref}, P_{HP}] = \frac{\rho}{\rho*}(c_1 + c_2T_e + c_3T_c + c_4f_{com} + c_5T_e^2 + c_6T_c^2 + c_7f_{com}^2 + c_8T_eT_c + c_9T_ef_{com} + c_{10}T_cf_{com} + c_{11}T_e^2f_{com} + c_{12}T_ef_{com}^2 + c_{13}T_c^2f_{com} + c_{14}T_cf_{com}^2 + c_{15}T_eT_cf_{com}) \quad (1)$$

where ρ^* is the compressor inlet density at nominal conditions; f_{com} represents the compressor frequency, T_e and Tc are the evaporation and condensation temperatures of the system, respectively.

Based on the measured data from circulation fan manufacturers, a data-driven model of circulation fan output power (P_{cf}) is constructed:

$$P_{cf} = 107.2\left(\frac{V_{air}}{V_{air}^*}\right)^3 - 175.6\left(\frac{V_{air}}{V_{air}^*}\right)^2 - 130.5\left(\frac{V_{air}}{V_{air}^*}\right)^1 - 59.39 \quad (3)$$

where, V_{air}* and V_{air} represents the rated and actual circulating airflow of the circulating fan, respectively.

2.2.2. Finned tube heat exchanger model

This study developed distributed parameter models (DPM) for the evaporator and condenser, as illustrated in Fig. 2, The hot and cold media within the heat exchanger are arranged in an overall counterflow configuration. During the modeling process, the domain is discretized into grids along the refrigerant flow direction. The outlet state of the refrigerant from one grid within the tube serves as the inlet state for the subsequent tiny cell. At elbow bends and connection points between different tube rows, grids are sequentially linked.

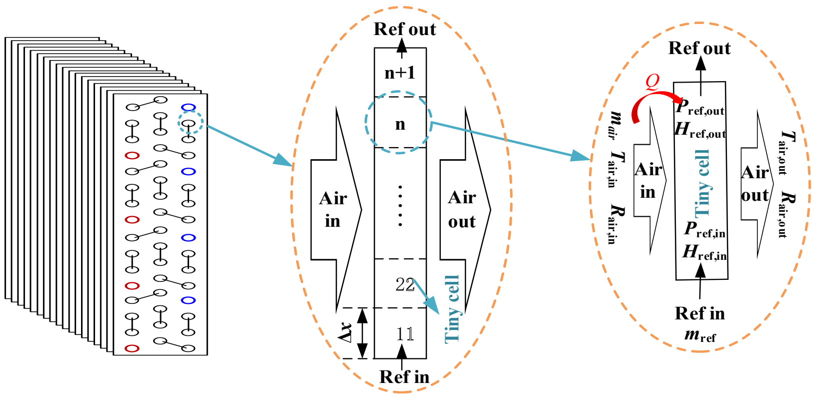

Figure 2. Heat exchanger grid division based on DPM

The forced convection heat transfer coefficient of humid air outside the tube is calculated as follows [11]:

$$\alpha_o = \frac{Nu\lambda_f}{D_{eq}} = \frac{C\lambda_f ReRe_{air}^n}{D_{eq}}\left(\frac{L_{air}}{D_{eq}}\right)^{\left(-0.28+\frac{0.08Re_{air}}{1000}\right)} \quad (4)$$

where λ_f is the thermal conductivity of the fin material, and D_{eq} is the characteristic length.

When the refrigerant in the tube is a two-phase boiling heat transfer process with heat absorption (evaporator), the heat transfer coefficient is calculated as follows [12]:

$$\alpha_{ref} = \alpha_l\left(G_1G_0^{G2}\left(25Fr_{ref}\right)^{G5} + G_3GB_0^{G4}F_{fl}\right)(-1.2351\chi + 1.2589) \quad (5)$$

where χ is the quality of two-phase flow, Other parameters are listed in Table 1.

Table 1. Formula 5 Values of coefficient variables

Parameter	G_1	G_2	G_3	G_4	G_5	F_{fl}
Value	1.136	0.9	667.2	0.7	0.3	1.0

When the refrigerant in the tube is a two-phase condensing heat transfer process with heat emission, the heat transfer coefficient is calculated as follows [13]:

$$\alpha_{ref} = 0.023\left(Re_{ref}\right)^{0.8}\left(Pr_{ref}\right)^{0.4}\frac{\lambda_{ref}}{D_i}\left[(1-\chi)^{0.8} + \frac{3.8\chi^{0.76}(1-\chi)^{0.04}}{P_{cond}/P_{crit}}\right] \tag{6}$$

2.2.3. Capillary tube model

As the throttling element of the heat pump system, which plays a role in creating differential pressure and controlling the flow of the system for the heat pump system. The refrigerant inside the capillary tube can be considered as an internal isenthalpic process, so only its pressure loss needs to be modeled:

$$\Delta P_{ct,tol} = \Delta P_{ct1} + \Delta P_{ct,2} + \Delta P_{ct,3} \tag{7}$$

where $\Delta P_{ct,1}$ represents the refrigerant pressure drop due to the sudden narrowing of the capillary inlet; $\Delta P_{ct,2}$ represents the along-travel resistance pressure drop of the refrigerant over the length of the capillary tube (L_{ct}); and $\Delta P_{ct,3}$ represents the refrigerant pressure drop due to the sudden widening of the capillary outlet.

2.2.4. Drying model for clothes in tumbler

In the tumbler, the evaporation rate of moisture from the surface of clothes is calculated as follows [14]:

$$m_{evap(1,2)} = \omega A_{clo}\frac{\rho_{c,v}}{0.622}\left(\mu W_{clo} - \left(W_{gt,in} + W_{gt,out}\right)/2\right) = \rho_{air}V_{air}\left(W_{gt,out} - W_{gt,in}\right) \tag{8}$$

where ω is the humid air mass transfer coefficient on the surface of the clothing and μ is the activity coefficient of water vapor on the surface of the clothes, $W_{gt,in}$ and $W_{gt,out}$ are the moisture content of the air entering and leaving the tumbler, respectively.

Within the drying chamber, a portion of the thermal energy from the air is absorbed by the clothing and tumbler (Q_{load}), while another portion is dissipated into the surrounding cabinet environment through the tumbler wall (Q_{loss}). The schematic diagram illustrating the energy balance within the drying room is shown in Fig. 3

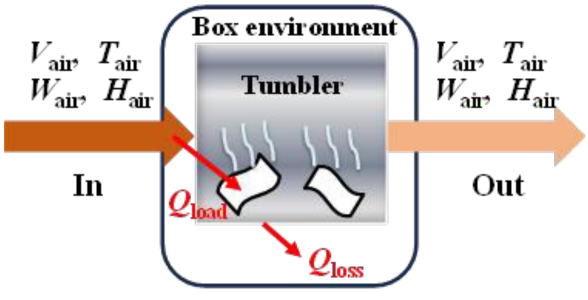

Figure 3. Energy balance in drying room

A time period (Δt), the energy balance equation for the drying chamber can be expressed as:

$$T_{clo,t+\Delta t} = T_{clo,t} + \left(\frac{\rho_{air}V_{air}\left(H_{gt,in}-H_{gt,out}\right)-Q_{loss}+m_{evap}H_{w,f}}{M_{clo}Cp_{clo}+XM_{clo}Cp_{water}+M_D Cp_{gt}}\right) \tag{9}$$

The power consumption required to drive the tumbler rotation is correlated with the total cloths weight which can be approximated as:

$$P_{gt} = -0.6761M_{clo,tol}^2 + 32.68M_{clo,tol} + 81.37 \tag{10}$$

2.2.5. Model solution method

This research puts forward a heat pump model solver for closed-cycle heat pump clothes dryers, which is based on a reverse enthalpy marching method coupled with an intelligent optimization algorithm. Particle Swarm Optimization (PSO) is chosen in this study for its strengths in fast convergence and strong robustness when dealing with medium- and low-dimensional continuous non-convex optimization problems. The reverse enthalpy marching method offers a new approach to solving problems related to closed heat pump clothes dryers. By establishing a new loss function and incorporating intelligent optimization algorithms, the solution of the system model is converted into a nonlinear constrained optimization problem. The formulation of the loss function is presented in Eq. 11, and results below 0.1 are regarded as convergent.

$$R(H_{com,in}, P_{com,out}, M_{ref}) = \sqrt{R(1) + R(2) + R(3)} \tag{11}$$

where $R(1)$, $R(2)$ and $R(3)$ are the basis loss functions generated during the implementation of the reverse enthalpy marching solution:

$$R_{tol}\begin{cases} R(1) = 0.5\left(H_{com,in} - H_{com,in-sim}\right)^2 \\ R(2) = 0.5\left(P_{com,out} - P_{com,out-sim}\right)^2 \\ R(3) = 0.5\left(M_{ref} - M_{ref,eva} - M_{ref,cond}\right)^2 \end{cases} \tag{12}$$

The drying chamber model is solved by the binary iterative method. The solution processes of the two models are illustrated in Fig.4. The overall performance of heat pump dryers is evaluated using the *MER* and *SMER*, calculated as follows:

$$\begin{cases} MER = M_{clo}(X_{start} - X_{end})/t_{tol} \\ SMER = M_{clo}(X_{start} - X_{end})/\sum\left(P_{HP} + P_{cf} + P_{gt}\right)\Delta t \end{cases} \tag{13}$$

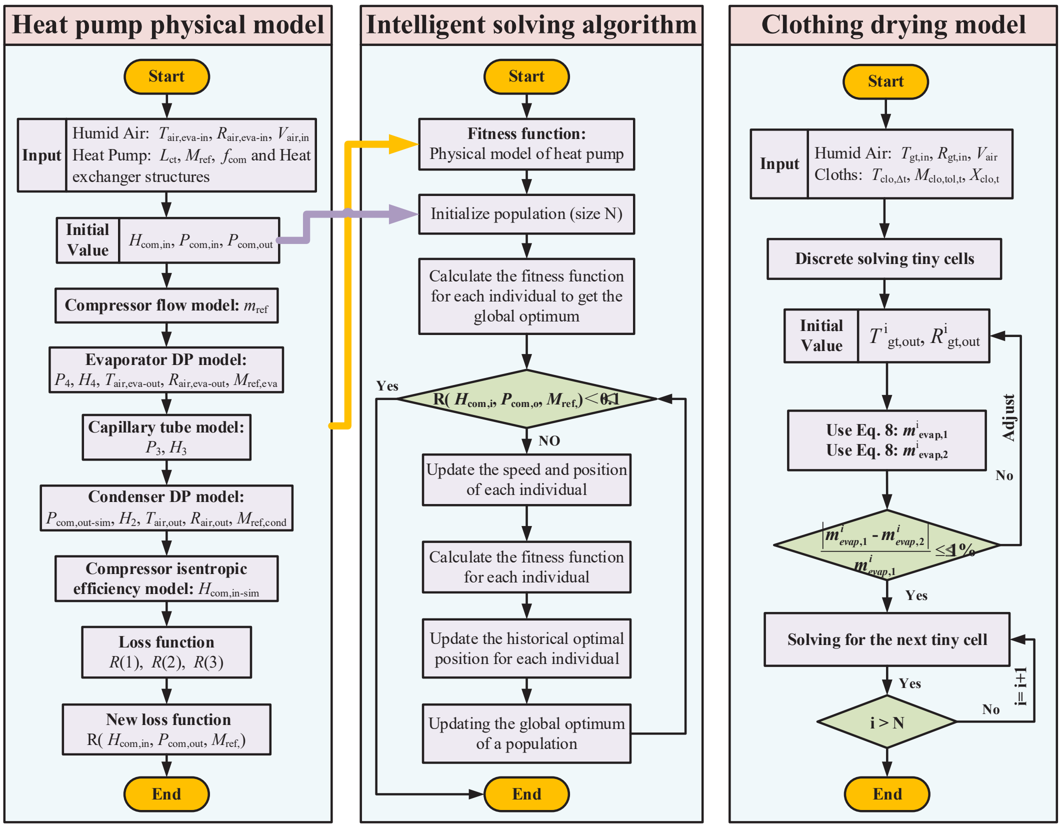

Figure 4. Solution process of the heat pump clothes dryer model

3. Experimental testing and model validation of heat pump clothes dryers

3.1. Prototype and experimental setup

This research conducts an experimental exploration of a closed-cycle heat pump tumble dryer system. As depicted in Fig. 5, the test prototype consists of core components: an evaporator, a compressor (model: HIGHLY PSA586DV-R3GJ5N), a condenser, a throttling element (i.e., a capillary tube), a circulating fan, and a dryer drum. R290 is adopted as the working medium for the heat pump system.

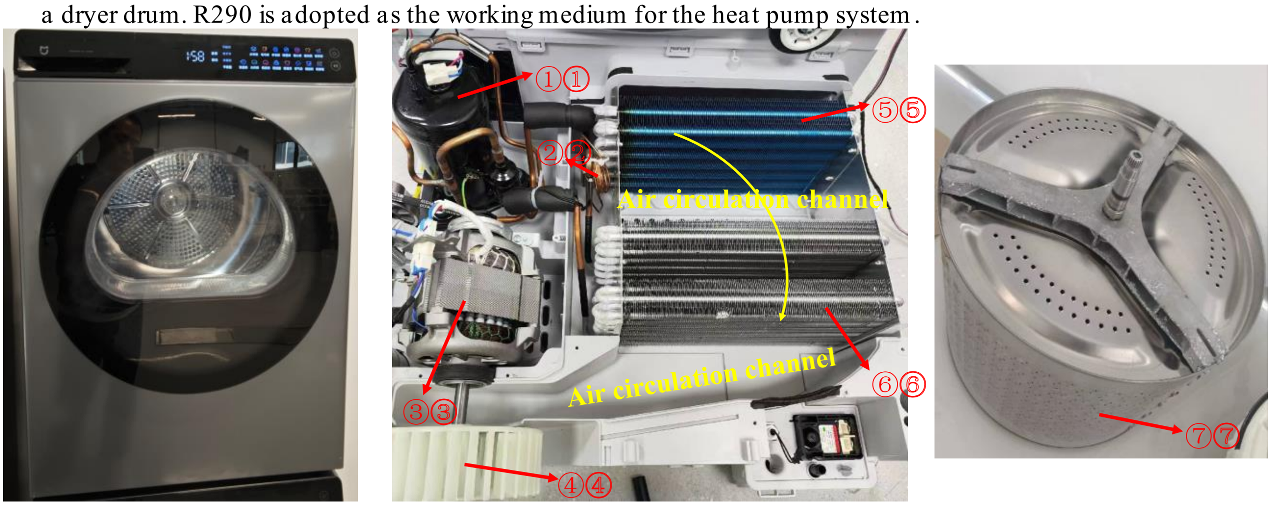

1. Compressor 2. Capillary tube 3. Fan motors 4. Fan impeller 5. Evaporator 6. Condenser 7. Dryer Tumbler

Figure 5. Experimental setup of the R290 closed-cycle heat pump tumble clothes dryer

The experimental prototype configuration was set as follows: compressor frequency was fixed at 50 Hz, the circulating fan's airflow rate was sustained at 184 m³/h, the capillary tube had dimensions of 0.9 × 700 mm, and the refrigerant charge was 0.14 kg. Critical structural parameters of the evaporator, condenser, and tumbler are compiled in Table 2. The test environment was maintained at a temperature of 22 (±0.1) °C and a humidity of 50 (±2%). The fabric was thoroughly soaked in water, with the initial moisture content regulated at 60% and the final moisture content at the end of drying set to 3%; all other testing conditions adhered to the specifications outlined in [15].

Table 2. Key structural dimensions of the components of the heat pump clothes dryer

Structures	Evaporator	Condenser	Tumbler structure	
Tube specification [51]	Φ 7 * (0.25 + 0.18)	Φ 7 * (0.25 + 0.18)	Cylinder diameter	580 mm
Tube type	Copper / Female threaded	Aluminium / Female threaded		
Row number	4	6	Cylinder height	339 mm
Tube number per row	6	6		
Tube pitch (mm)	21	21	Material	Stainless Steel
Row pitch (mm)	12.7	12.7		
Tube length (mm)	260	260	Weight	1930 g
Fin pitch (mm)	2.2	1.8		
Fin thickness (mm)	0.1	0.1	Specific Heat	490 J/(kg·K)
Fin type	Hydrophilic / Wave	Smooth / Louver		

3.2. Experimental testing and model reliability validation

Fig. 6 presents the validation results of the heat pump dryer system model under a benchmark load condition of 5 kg dry weight. As the drying process progresses, the inlet air temperature of the heat pump continues to rise. The outlet air temperature of the heat pump initially increases before stabilizing (with fluctuations). The evaporation temperature of the heat pump system first increases and then gradually decreases. The condenser outlet temperature initially rises and then remains stable.

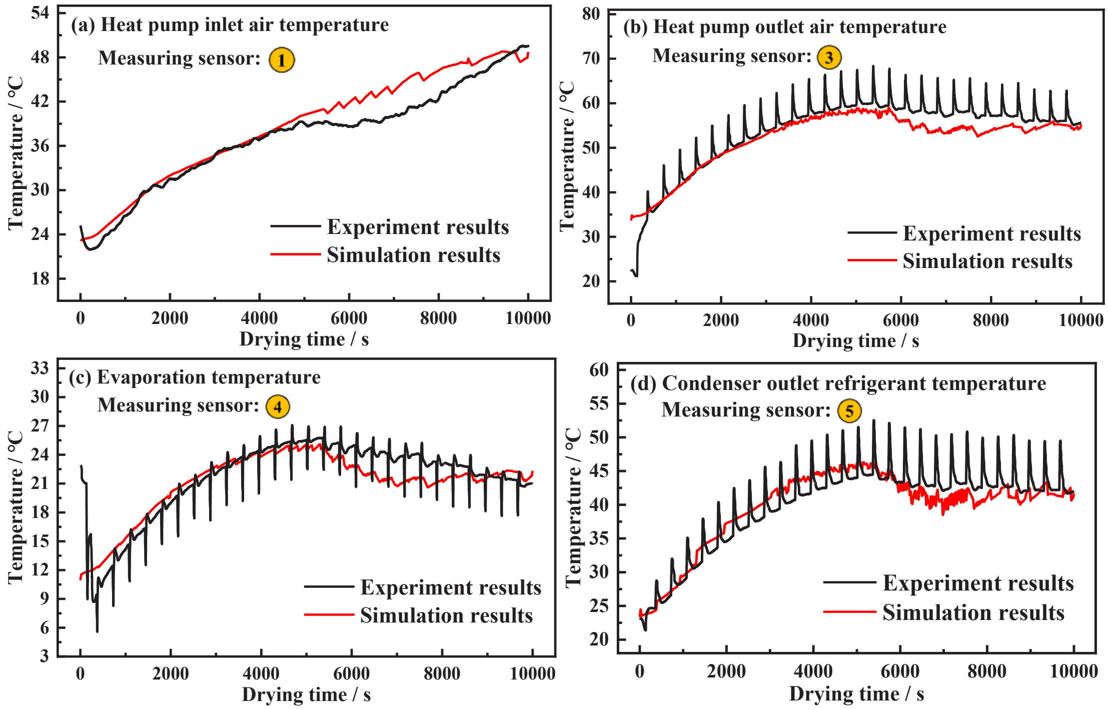

Figure 6. Experimental results are verified by the simulation model

Moreover, the model is verified to reliably predict the dynamic temporal variation characteristics of these variables throughout the drying process. It maintains high precision during the initial stage of drying but exhibits distinct fluctuations in the later stage. Aside from the inherent measurement deviations and cumulative computational errors in the heat pump clothes dryer model, the primary influencing factors are identified as the unstable heat dissipation from the air duct connecting the heat pump and tumbler to the external environment, along with the continuous variation in the internal ambient temperature of the dryer cabinet. The periodic forward/reverse rotation of the drum during the drying process affects the system's operational state, resulting in measurement spikes from the sensors. In summary, the heat pump clothes dryer model is capable of accurately reconstructing the drying process, with the maximum temperature prediction deviation not exceeding 4.3 K and the average deviation being less than 0.5 K.

4. Simulation modeling results and discussion

4.1. The heat and moisture transfer process of clothing

Fig. 7 illustrates the effects of changes in air supply conditions (a) and clothing moisture content (b) on the drying process, where ΔT refers to the change in clothing temperature (K) within 20s. It can be observed that as the air volume flow rate increases, the moisture evaporation rate of the clothing gradually rises, and the temperature rise of the clothing during the drying cycle also increases progressively. This is because an increase in air volume flow rate leads to greater energy input into the drying chamber; simultaneously, the enhanced air velocity improves the convective heat transfer coefficient and mass transfer coefficient between the hot air and the clothing, thereby increasing the clothing's temperature rise and moisture evaporation rate.

From Fig. 7 (b), under constant air supply conditions, as the clothing moisture content decreases, the clothing's temperature rise gradually increases, while the moisture evaporation rate decreases. This is attributed to two factors: first, a reduction in clothing moisture content lowers the total clothing weight (dry weight plus moisture weight), leading to a faster temperature rise of the clothing with the same hot air energy input; second, as the moisture content decreases, the proportion of free water on the clothing surface diminishes, with most of the remaining water trapped between the clothing fibers, making moisture evaporation more difficult.

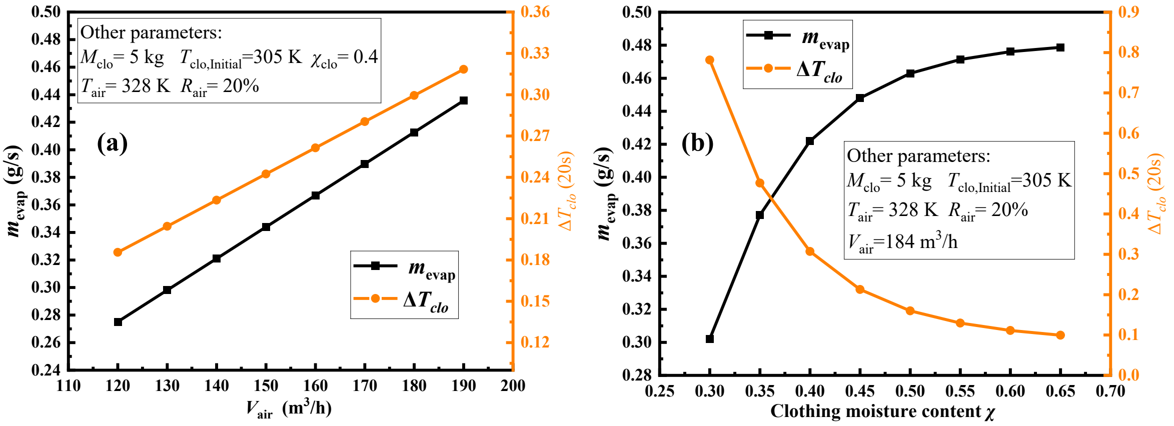

Figure 7. Effects of parameter variations on the drying process: (a) *V*air (b) Clothing moisture content

4.2. Operating parameters effect on dryer performance

Fig. 8 illustrates the impact of compressor operating capacity on the performance of the clothes dryer, where the strength of the compressor's operating capacity is reflected by changes in its operating frequency. As shown in Fig. 8 (a), with the increase in compressor frequency, the *MER* gradually increases, while the Specific *SMER* first increases and then decreases. From Fig. 8 (b), it can be observed that as the compressor frequency rises, the moisture evaporation rate on the clothing surface gradually increases, which is the primary reason for the increase in the dryer's *MER*. In addition, an increase in compressor frequency leads to higher power consumption of the heat pump, but shortens the drying time. The electrical energy consumed throughout the entire drying cycle does not change monotonically. Therefore, there theoretically exists an optimal compressor operating frequency that minimizes the total power consumption of the dryer during the entire cycle and maximizes the *SMER*.

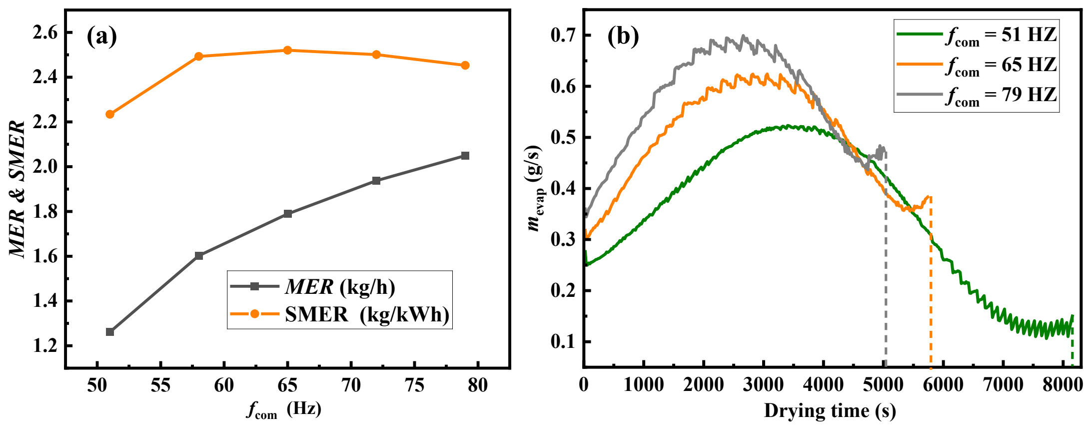

Figure 8. Effect of compressor frequency variation on dryer performance

Fig. 9 illustrates the influence of variations in the circulating air volume flow rate of the fan on the performance of the clothes dryer. As shown in Fig. 9 (a), within the test range, with the increase in the fan's circulating air volume flow rate, the *SMER* gradually increases, while the *MER* gradually decreases. From Fig. 9 (b), it can be observed that as the circulating air volume flow rate increases, the drying time progressively extends; in the early stage of drying, a larger air volume flow rate results in a higher m_{evap}, but in the later stage of drying, it leads to a decrease in m_{evap}. This phenomenon is attributed to the mismatch between the larger circulating air volume flow rate and the operating capacity of the heat pump. A larger air volume flow rate prevents the evaporator from meeting the dehumidification demand at that air volume flow rate, and also impairs the heating capacity of the condenser. This causes the temperature of the clothing in the drum to rise slowly and the moisture evaporation rate per unit time of the clothing to decrease, which is the reason for the gradual reduction in *MER*. In addition, the larger the circulating air volume flow rate, the lower the overall power consumption of the dryer (Primarily due to the increase in circulating air volume flow rate, the system's evaporation and condensation temperatures decrease, thereby reducing the energy consumption of the heat pump (compressor)). Therefore, although the drying time increases slightly, the total electrical energy consumption of the dryer during the entire drying cycle decreases, thus leading to a gradual increase in *SMER*.

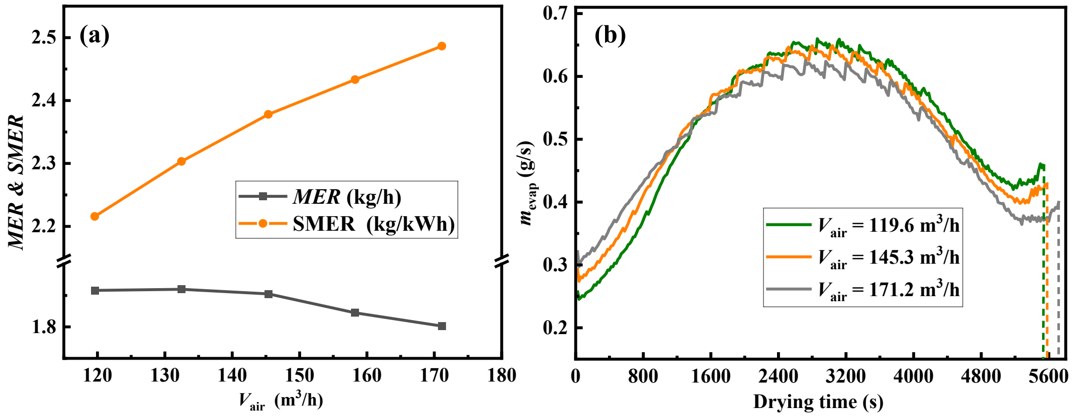

Figure 9. The effect of circulating air volume flow rate changes on dryer performance

5. Conclusions

This research conducted simulation analysis, experimental testing, and optimization studies on an R290 closed-cycle heat pump tumble dryer, yielding the following key conclusions:

- A comparison with experimental data from the prototype reveals that the dryer's quasi-steady-state simulation model achieves a maximum temperature prediction error of no more than 4.3 K, with the average temperature prediction error remaining under 0.5 K.
- As the circulating air volume flow rate increases, both the temperature rise of the laundry inside the drum and the rate of moisture evaporation increase. As the moisture content of the laundry rises, the temperature increase within the drum gradually decreases while the rate of moisture evaporation progressively increases.
- Optimizing compressor frequency boosts *MER* by 62.9% (1.26→2.05 kg/h) and *SMER* by 13.0% (2.23→2.52 kg/kWh). Within the test range, the *MER* decreases with increasing V_{air} (1.80→1.86 kg/h), while the *SMER* increases with increasing V_{air} (2.21→2.49 kg/kWh).

Nomenclature

Latin symbols		λ	Thermal conductivity, W/(m·K)
A	area, m^2	δ	Thickness, m
D	diameter, m	α	convective heat transfer coefficient, W/(m^2·K)
f	frequency, Hz	**Subscripts and Superscripts**	
L	length, m	cf	circulation fan
m	mass flow rate, kg/s	clo	cloth
M	mass, kg	com	compactor
P	pressure, Pa	c/cond	condenser
R(i)	loss function	ct	capillary tube
T	temperature, K	e/eva	evaporator
t	time, s	gt	tumbler
V	air volume flow rate, m^3/h	*tol*	total
W	air humidity content, g/kg	**Abbreviations**	
X	water content of clothes	DPM	distributed parameter model
Greek symbols		*MER*	moisture extraction rate
μ	activity factor	PSO	particle swarm optimization
ρ	density, kg/m^3	*Re*	Reynolds number
ω	mass transfer coefficient, m/s	*SMER*	specific moisture extraction rate

Acknowledgements

The authors would like to acknowledge the financial supports from Technological Innovation Program Project of Hubei Province (2024BAB102), National Natural Science Foundation of China (No. 52076085) and Program for HUST Academic Frontier Youth Team (No. 2019QYTD10).

References

[1]. Bansal P, Vineyard E, Abdelaziz O. Advances in household appliances-A review. Applied Thermal Engineering, 2011, 31(17-18): 3748-3760.
[2]. Liu Y, Shao S. Experimental Study on Energy Efficiency of Heat Pump Clothes Dryer with Natural Refrigerant R290. Journal of Refrigeration, 2021, 199: 117545.
[3]. IEA, Residential Energy Consumption Survey (RECS), Dept. of Energy, U.S. (2017).
[4]. Colak N, Hepbasli A. A review of heat pump drying: Part 1–Systems, models and studies. Energy conversion and management, 2009, 50(9): 2180-2186.
[5]. Heath E A. Amendment to the Montreal protocol on substances that deplete the ozone layer (Kigali amendment). International Legal Materials, 2017, 56(1): 193-205.
[6]. Ibrahim OAAM, Kadhim S A, Hammoodi K A, et al. Review of hydrocarbon refrigerants as drop-in alternatives to high-GWP refrigerants in VCR systems: the case of R290. Cleaner Engineering and Technology, 2024: 100825.
[7]. Dai B, Zhao P, Liu S, et al. Assessment of heat pump with carbon dioxide/low-global warming potential working fluid mixture for drying process: Energy and emissions saving potential. Energy Conversion and Management, 2020, 222: 113225.
[8]. Shen B, Nawaz K, Elatar A. Parametric studies of heat pump water heater using low GWP refrigerants. International Journal of Refrigeration, 2021, 131: 407-415.
[9]. Joudi K A, Al-Amir Q R. Experimental Assessment of residential split type air-conditioning systems using alternative refrigerants to R-22 at high ambient temperatures. Energy conversion and management, 2014, 86: 496-506.
[10]. Household and similar electrical appliances-Safety-Part 211: Particular requirements for tumble dryers: IEC 603352-11:2019. Switzerland: International Electrotechnical Commission,2019.
[11]. Faghri A, Zhang Y, Howell J R. Advanced heat and mass transfer. Global Digital Press, 2010.
[12]. Kandlikar S G. A general correlation for saturated two-phase flow boiling heat transfer inside horizontal and vertical tubes. 1990.
[13]. Kandlikar S G, Alves L. Effects of surface tension and binary diffusion on pool boiling of dilute solutions: an experimental assessment. 1999.
[14]. Li J, Yan X, Zhang M, et al. Simulation and analysis of a new cabinet heat pump clothes dryer. International Communications in Heat and Mass Transfer, 2023, 143: 106688.
[15]. Tumble dryers for household use - methods for measuring the performance: EN 61121:2013. Brussels: European Committee for Electrotechnical Standardization,2013.